Natural Rubber Latex LbL Films: Characterization and Growth of Fibroblasts

Christiane P. Davi,[1] Luiz F. M. D. Galdino,[1] Primavera Borelli,[2] Osvaldo N. Oliveira, Jr.,[3] Mariselma Ferreira[1]

[1]*Laboratório de Eletroquímica e Materiais Nanoestruturados, Universidade Federal do ABC, Santo André-SP, Brazil*
[2]*Departamento de Farmacologia, Universidade de São Paulo, São Paulo, SP, Brazil*
[3]*Instituto de Física de São Carlos, Universidade de São Paulo, São Carlos, SP, Brazil*

Received 23 May 2011; accepted 8 October 2011
DOI 10.1002/app.36309
Published online 20 January 2012 in Wiley Online Library (wileyonlinelibrary.com).

ABSTRACT: The recent biomedical applications of natural rubber (NR) latex, mostly in dry membranes, have motivated research into novel, more noble uses of this low-cost biomaterial. In this article, we provide the first report on the fabrication of layer-by-layer (LbL) films of NR alternated with the polyelectrolytes polyethylenimine (PEI) and polyallylamine hydrochloride (PAH). Stable $(PAH/NR)_n$ and $(PEI/NR)_n$ LbL films displayed similar physicochemical properties, but differed in terms of film morphology according to atomic force microscopy (AFM) and scanning electron microscopy (SEM) data. Most significantly, $(PEI/NR)_5$ LbL films were made of smaller and flattened particles, which were not efficient for the growth and proliferation of normal human fibroblasts (NHF). In contrast, efficient NHF proliferation could be obtained with $(PAH/NR)_n$ LbL films, with the fibroblasts exhibiting the expected elongated morphology. Furthermore, cell growth did not occur for cast films of NR, thus demonstrating the suitability of the LbL method for this biologically related application. The differences between the two polyelectrolytes illustrate the importance of the film architecture and morphology, which open the way for exploiting the molecular control inherent in the LbL technique for further applications of NR-containing films.
© 2012 Wiley Periodicals, Inc. J Appl Polym Sci 125: 2137–2147, 2012

Key words: biomaterials; interfaces; rubber; films

INTRODUCTION

Natural rubber (NR) is an important raw material for various products, including tires, surgical gloves, condoms, and pillows.[1] Biomedical applications have been demonstrated in recent years, as NR has the ability to induce wound healing,[2–5] angiogenesis,[6] and tissue regeneration.[3–5] NR has also been used in sensors,[7] drug delivery matrices,[5,8] and vascular prosthesis.[9,10] The clinical use of NR latex[11–13] and proteins extracted from the serum[14,15] is well established for treating chronic skin ulcers,[3,11] in which NR is normally used as extracted from the tree or stabilized with ammonia. Interestingly, using NR as biomaterial seems inconsistent with the well-documented, widespread occurrence of allergies.[16–20] In fact, allergies associated with NR products are caused by the residual proteins[17,20,21] or other chemical compounds, e.g. vulcanizing agents, used in the processing. Nevertheless, the same latex serum containing the proteins, and therefore all allergens, can also heal wounds and express angiogenic activity.[6,14,15,22] Therefore, this apparently paradoxical behavior means that many possibilities of applications and research are still to be explored with NR.

The products and applications mentioned above employ NR in the form of either vulcanized elastomers or dry latex membranes. To our knowledge, the use of NR in its colloidal form has not been reported and represents further opportunities. One possibility is to fabricate nanostructured films from the colloidal NR dispersions, which was the strategy we adopted here with the layer-by-layer (LbL) technique.[23] This method is based on the adsorption of alternating layers of positive and negatively charged materials and has been exploited to produce interfaces for cell cultures[24–28] and co-cultures,[29] as it allows the surface characteristics to be controlled and the cells adhesion be mediated.[30,31] LbL films were used for controlled release of growth factors[32–34] that may also induce cells proliferation and angiogenesis. Because NR latex particles are negatively charged, we alternated NR layers with the polycations poly(ethylenimine) (PEI) and poly(allylamine) hydrochloride (PAH). In addition to investigate their physicochemical properties, we used these films as surfaces for proliferation of human fibroblasts.

Correspondence to: M. Ferreira (mariselma.ferreira@ufabc.edu.br).

© 2012 Wiley Periodicals, Inc.

EXPERIMENTAL

Film fabrication

NR latex has been extracted from the *Hevea brasiliensis* tree, clone RRIM600, kindly donated by *Embrapa*, containing 30–45% of *cis*-1,4-polyisoprene, 4–5% of nonrubber constituents (proteins, lipids, carbohydrates, salts, sugars, etc.), and 50% of water.[35,36] The NR particles have sizes ranging from 5 nm to 3 μm, normally with spherical shapes made of *cis*-polyisoprene.[36] The particles are kept stable on the latex colloidal system because phospholipids surround them which also render the particles surface negatively charged.[36,37] NR was employed as received without centrifugation and preserved with 1% of NH_4OH. A dilute solution of NR (2.5 μL L^{-1}, pH 9.0) was freshly made and used without storage. The LbL films were built by alternating layers of NR latex with polycationic layers of either PEI or PAH. Solutions of PEI (1.0 mg mL^{-1}, Aldrich, MW 25,000 g mol^{-1}) and PAH (0.5 mg mL^{-1}, Aldrich, MW 56,000 g mol^{-1}) were made to pH 6.0 using Milli-Q water. Other solutions had specific use in the characterization and will be described together with the methodology. The adsorption time for each layer was 3 min, and after depositing each layer, the substrate + film system was rinsed in Milli-Q water at the same pH of the previous solution, and dried with a nitrogen flow. LbL films with 5, 10, 15, and 20 bilayers were obtained depending on the characterization method. The substrates for LbL film deposition were cleaned as follows: (i) Quartz (30 mm × 10 mm × 1 mm) and glass substrates (1.5 cm^2) were boiled for 10 min in a basic solution (NH_4OH, H_2O_2, H_2O, 1:1:5, v/v), then rinsed in Milli-Q water. Finally, the substrates were rinsed once again. This cleaning assures the presence of negative charges on the surfaces, which were kept free from organic molecules. (ii) Gold substrates (30 mm × 20 mm × 1 mm) were cleaned by immersion in organic solvents (butanone and ethanol). (iii) Mica substrates (1.5 mm^2) were obtained with removal of the uppermost layer with an adhesive tape.

For the dimethyl thiazol diphenyl tetrazolium bromide (MTT) assays, cast films were produced with the same solutions to compare with the LbL films. Casting was performed by allowing 100 μL of PEI, PAH, and NR solutions to dry on culture polystyrene wells.

Film characterization

We used UV–vis spectroscopy (Cary 50, Varian) to monitor the construction and degradation process in films deposited on quartz substrates, with the absorption at 200 nm being measured every two cycles of deposition up to a total of 10 cycles. All multilayer films were produced in triplicate at room temperature. Degradation tests (ASTM F1635-04a) were done by immersing the sample films in 5 mL of phosphate buffer solution (PBS) at pH 7.4, and kept at 37°C for 21 days. Periodically the samples were taken off the PBS solution, dried and reanalyzed at 200 nm in intervals of 12 h on the first 2 days, 24 h until the sixth day, and 48 h until the 21st day. To avoid contamination, the PBS solution was constantly replaced. Clean quartz substrates, submitted to the conditions above, were used as control.

For the FTIR measurements, $(PEI/NR)_{20}$ and $(PAH/NR)_{20}$ LbL films were adsorbed on gold substrates. Cast films were made by allowing drops of each solution to dry over the substrate. All samples were dried at 37°C for 3 h prior to the analysis to avoid interference of the water OH groups. ATR-FTIR measurements were made using a Thermo-Nicolet, model Nexus 470 spectrometer in a N_2 atmosphere. Images of scanning electron microscopy (Digital Scanning Microscope, DSM 960, Carl Zeiss), with 20 kV e-beam at 10^{-5} mmHg, were performed in films adsorbed on glass substrates. Analogously to any other non-conductive sample, the films had to be coated with gold (Sputter Coater SCD 059, Oerlinkon Balzers) prior to the measurements.

Atomic force microscopy (SPM5.500, Agilent Technologies) was used in the contact mode to study the morphology of films deposited on mica substrates. A silicon tip and cantilever with spring constant of 0.2 N m^{-1} were used to scan areas of 10×10, 30×30, 50×50, and 75×75 μm of the film surface. The AFM images were treated with the Gwyddion (v.2.16) software to correct lines, horizontal scars, plane and polynomial background, in this order. Those images were used to analyze surface roughness, grain statistics, and the profile of the particles topology. These analyses were made using an average of all the AFM data. The root mean square (Rms) roughness was determined in three steps: (i) 15 points logarithmically spaced in the scan size scale (2–75 μm) were calculated; (ii) these points were used as zoom areas, focusing on the upper left, middle and bottom right side of the images; (iii) Rms roughness was measured at all points and the mean data plotted as ln(Rms × scan size) giving the roughness on stable regions. The grain statistics analysis tool of the Gwyddion software was used to find the mean particle size, volume, and percentage of film surface coverage. The profiles of the particles topology were obtained, with the length and height (at the middle length) being compared to assess the particles shape. Six particles were chosen randomly and analyzed. We consider particles as flat when the length was at least 20 times their height.[37] Contact angle measurements were made after deposition of each layer up to nine layers for $(PEI/NR)_n$ and $(PAH/NR)_n$ films.

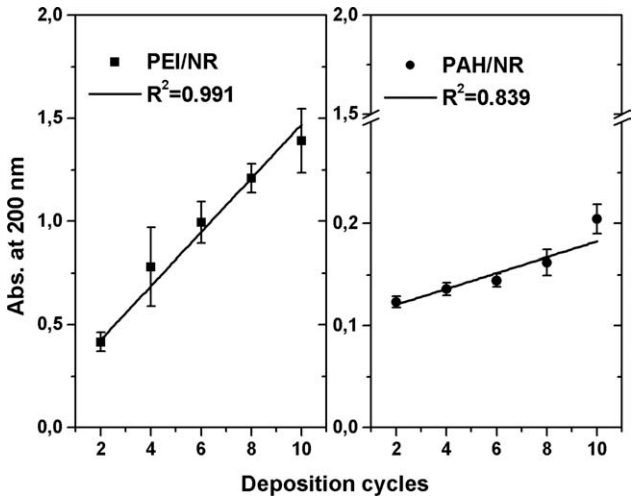

Figure 1 Construction of PEI/NR and PAH/NR films. Material depositions detected by UV–vis for each two deposition cycles.

For the films with odd numbers of layers, the topmost layer was made with PEI or PAH, while latex was in the topmost layer for the even numbers. The contact angles were determined on a 10 μL Milli-Q water droplet, gently placed onto the surface. The angles were calculated with the Surftens (v.3.0) software using the images taken with a CCD camera (LG Electronics). All experiments were conducted at room temperature using a homemade apparatus.

Cells proliferation – dimethyl thiazol diphenyl tetrazolium bromide (MTT) assay

We used normal human fibroblasts (NHF), kindly donated by Dr. Fabio Forti from Instituto de Química, USP (Brazil). The number of NHF was determined by colorimetric quantification with MTT. NHF were cultivated directly on $(PEI/NR)_5$ and $(PAH/NR)_5$ to evaluate the influence of the multilayer films on cell proliferation. The polystyrene surface of culture wells was used as blank control, and cast films made with PEI, PAH or NR solutions were analyzed for comparison. In total, 27 replicates (nine for each day of tests) of the control surface and each type of film (cast and LbL) were fabricated on culture plates of 24 wells. Six of these replicates received 10^3 cells cultured with 90% of Dulbecco's modified Eagle's medium (DMEM) and 10% fetal calf serum (FCS) at 37°C in 5% of CO_2. Three replicates received only the culture medium, without cells, to discount possible interference of samples in the colorimetric method. The measurements under the conditions above were repeated to determine the NHF number for 7, 14, and 21 days of cultivation. All NHF cultures were photographed prior to MTT quantification using a CCD camera connected to an inverted optical microscope (Eclipse TS-100, Nikon Instruments).

The MTT quantification method was as follows. All culture plate wells received 100 μL of MTT (5 mg mL^{-1}) reagent and were kept at 37°C for 4 h to ensure the formation of formazan crystals inside the viable cells. Then the wells received 1 mL of sodium dodecyl sulfate (50 mg mL^{-1} in 0.01 M HCl) kept for 24 h for color release. Absorbance measurements at 570 nm were made on three aliquots of 200 μL of each medium by ELISA (EL800-Universal Microplate Reader, Bio Tek Instruments). A calibration curve was obtained to correlate the measured absorbance with the number of cells.

Cells morphology

The NHF morphology was further analyzed with SEM images (LEO 440 with Oxford detector, Leica-

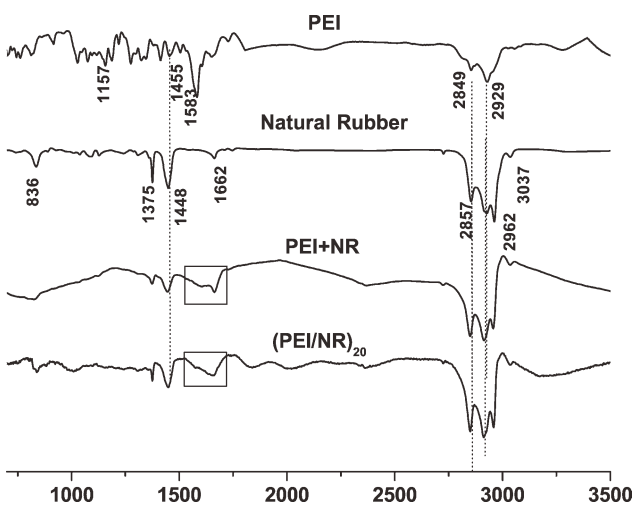

Figure 2 FTIR spectra for $(PEI/NR)_{20}$ LbL films and cast films of PEI and NR and mixture of PEI + NR.

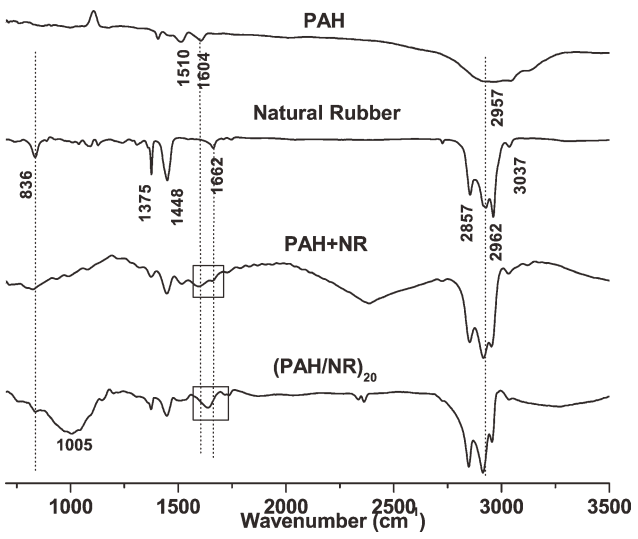

Figure 3 FTIR spectra for $(PAH/NR)_{20}$ LbL films and cast films of PAH and NR and mixture of PAH + NR.

TABLE I
List of Assignments for the Main Functional Groups of NR, PEI, and PAH Identified by FTIR

NR		PEI		PAH	
Wavenumber (cm^{-1})	Assignment[37,39,40]	Wavenumber (cm^{-1})	Assignment[41]	Wavenumber (cm^{-1})	Assignment[42]
836	C=CH wagging				
		1122	C—N stretching		
1375	C—H bending of CH_3				
1448	C—H bending of CH_2	1453	Inplane bending of CH_2		
				1510	N—H bending
		1583	NH vibration		
				1604	N—H bending
1662	C=C stretching				
2857	C—H stretching of CH_2 and CH_3	2849	Symmetric vibration of CH_2		
2927	C—H stretching of CH_2	2929	Asymmetric vibration of CH_2	2957	NH_3 stretching
2962	C—H stretching of CH_3				
3037	.=CH stretching in (C(CH_3=CH)				

Zeiss) using a 20 kV e-beam. The images were taken after the NHF were fixated, and then coated with gold (MED020, BAL-TEC coating system). For SEM analysis, 10^3 NHF were cultivated (DMEM at 37°C, 5% CO_2) for 3 days on $(PEI/NR)_5$ and $(PAH/NR)_5$ films. The samples were deposited on round glass substrates (1.5 cm^2), later placed inside the culture wells. Cells were fixated after the cultivation medium was redrawn, as follows: On each sample, 1 mL of a solution of 55% Tris–HCl buffer (at pH 7.2), 40% paraformaldehyde (25:1, v/v), and 5% glutaraldehyde (33:1, v/v) was added. This solution was redrawn after 2 h at room temperature and cells were dehydrated with ethanol. Dehydration begun with 1 mL of ethanol 30% for 10 min, continuing with solutions of higher concentration gradients (50,

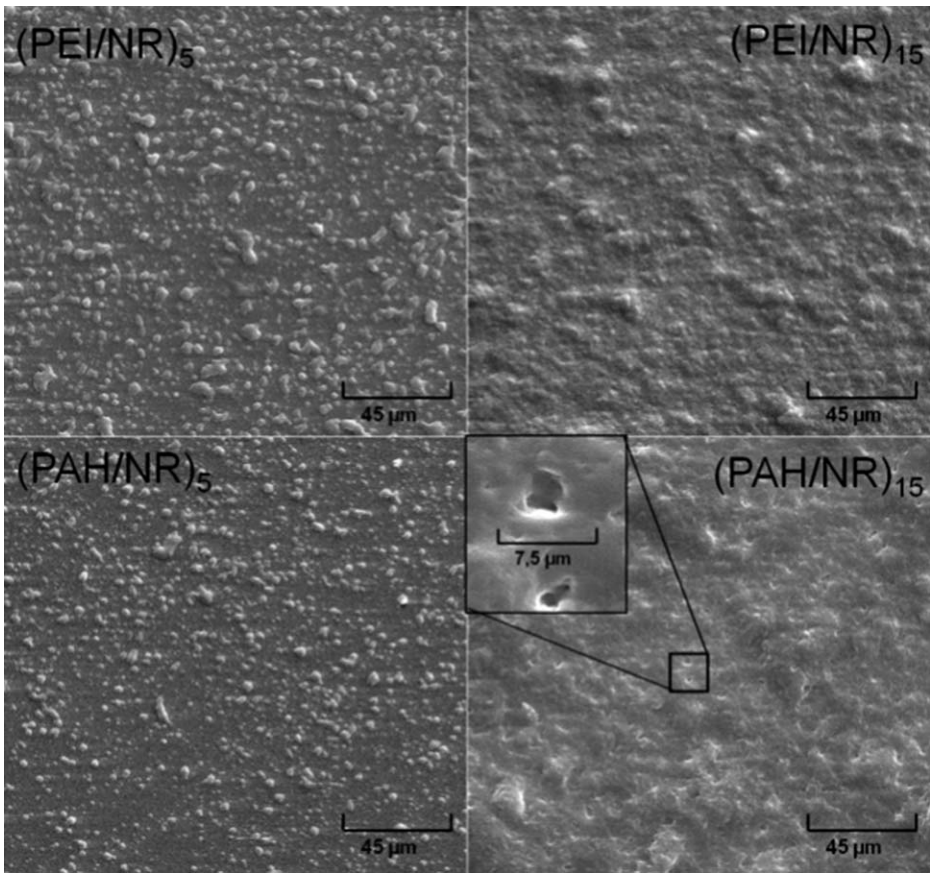

Figure 4 SEM images for the LbL films with the following architectures: $(PEI/NR)_5$, $(PEI/NR)_{15}$, $(PAH/NR)_5$, and $(PAH/NR)_{15}$. The insert in the bottom right figure shows cavity-like structures.

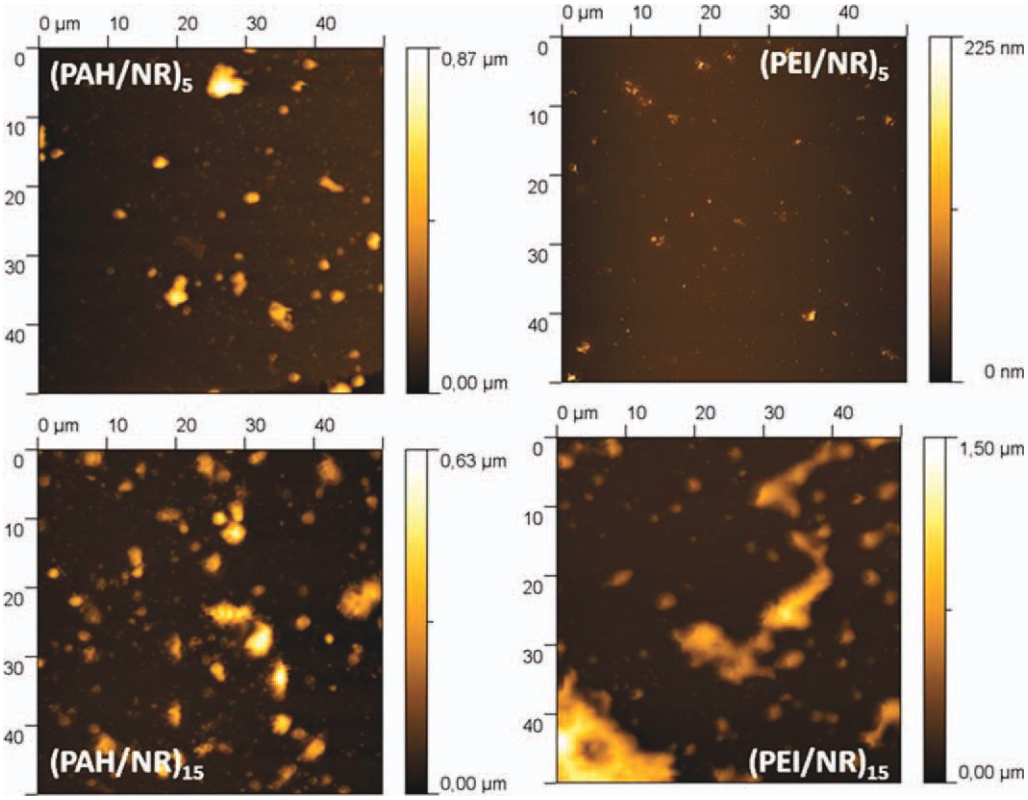

Figure 5 AFM images of PEI/NR and PAH/NR films with different numbers of bilayers. [Color figure can be viewed in the online issue, which is available at wileyonlinelibrary.com.]

70, 90, 100%). In addition, samples were covered with absolute ethanol and hexadimethyl silazane (HDMS – 98%, CAS: 999-97-3, Acros Organics) 1:1 (v/v) for 10 min. Finally, the sample received 500 µL of HDMS that were allowed to dry at room temperature.

RESULTS AND DISCUSSION

NR-containing LbL films

A linear increase in absorbance with the number of bilayers was observed in the buildup of the $(PEI/NR)_{10}$ and $(PAH/NR)_{10}$ LbL films, as shown in Figure 1, thus indicating that the same amount of material was deposited in each cycle. Also shown is that a more effective adsorption took place for $(PEI/NR)_{10}$. We investigated the film stability by immersing the LbL films into a PBS solution. For a few days, the light absorption of the films increased, probably owing to swelling,[38] but after 20 days the absorption returned to a value close to the initial one, which demonstrates that the LbL films are stable (results not shown).

The adsorption of the polyelectrolytes and NR was confirmed with the FTIR spectra of Figures 2 and 3, which feature the main bands assigned to functional groups of the film components, as indicated in Table I. Significantly, the spectra for the $(PEI/NR)_{20}$ and $(PAH/NR)_{20}$ LbL films are not the mere superimposition of the spectra of the individual components. For instance, a broad band enclosed by a square in Figure 2 encompasses the 1662 cm^{-1} C=C stretching from the NR chain and the 1583 cm^{-1} NH vibration of the PEI chain. The broad band is not the superimposition of the latter, thus pointing to molecular level interactions between PEI and NR in the $(PEI/NR)_{20}$ film, probably associated with electrostatic interactions involving the NH group. As for the $(PAH/NR)_{20}$ LbL film, again the band assigned to the NH group in PAH was affected by the interaction with NR, with the same bands described for the $(PEI/NR)_{20}$ film appearing. Bands were observed at 836, 1375, 1448, 2857, and 3037 cm^{-1}, assigned to the NR chain. The band marked with a dotted line in Figure 3 indicates interaction

TABLE II
Particles Data Analysis

Sample	Mean size (µm)	Total volume ($µm^3$)	Surface coverage (%)
$(PEI/NR)_5$	0.3	63	4.6
$(PEI/NR)_{15}$	0.9	159	18.0
$(PAH/NR)_5$	0.3	138	8.0
$(PAH/NR)_{15}$	1.1	625	16.0

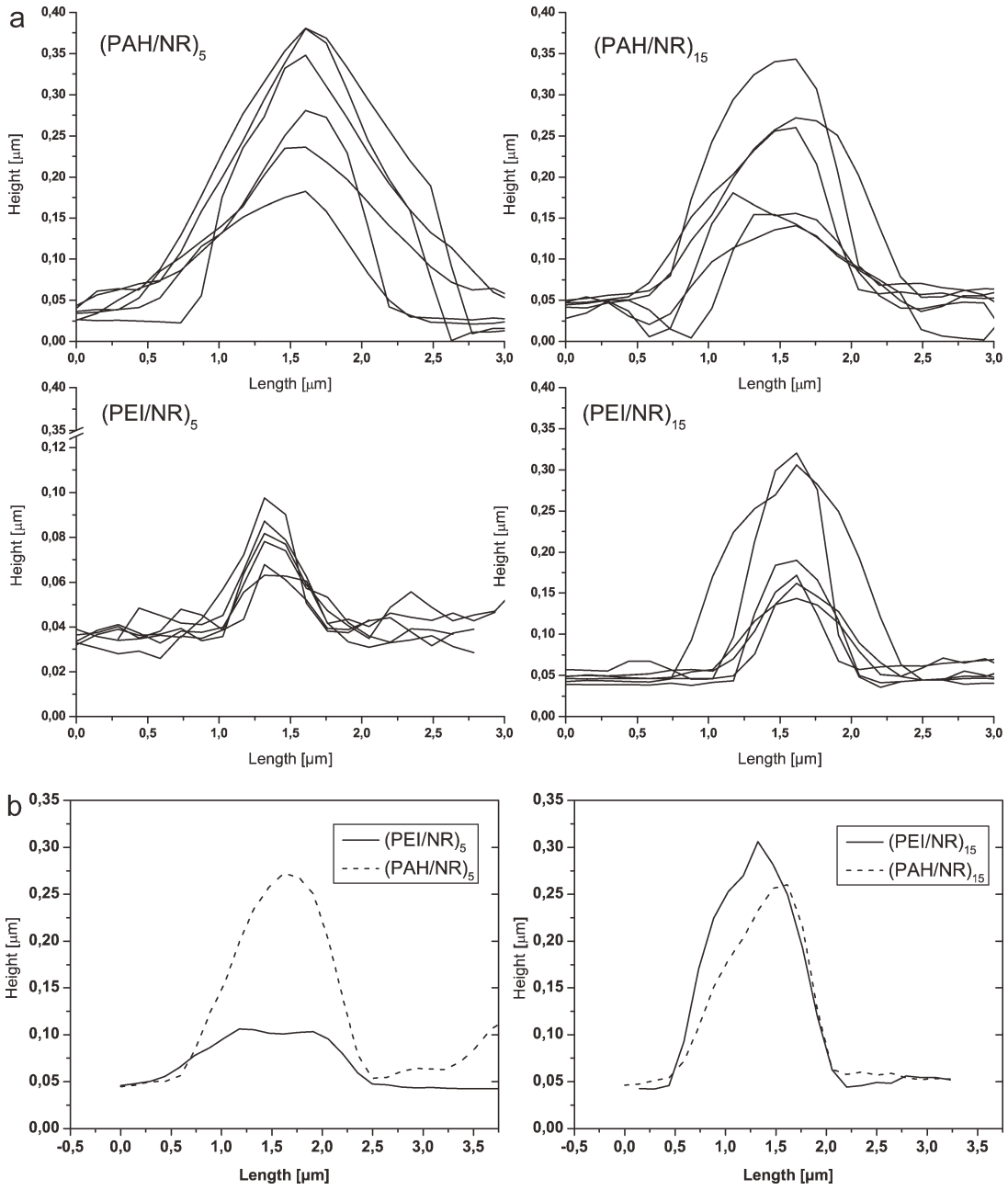

Figure 6 a: Line profile of NR particles with length around 2.0 μm. b: Line profile of NR particles for 5- and 15-bilayer PEI/NR and PAH/NR films.

between the (2957 cm^{-1}) NH_3 stretching of PAH and the (2927 cm^{-1}) C—H stretching of the NR chain. In Figure 3, the band marked within a square is in the NH vibration region at 1604 cm^{-1} for PAH, while the one at 1662 cm^{-1} is assigned to the C=C stretching of the NR chain. The band at 1510 cm^{-1} for the N—H bending identified by an arrow is assigned to PAH alone. Therefore, most of the bands in the $(PAH/NR)_{20}$ spectra denote electrostatic interaction between PAH and NR. However, the appearance of a broad band at 1005 cm^{-1} in the $(PAH/NR)_{20}$ LbL film, and absent in the PAH + NR mixture, suggests other interactions. This should be expected because NR is such a complex biomaterial, e.g., containing proteins that may interact via hydrogen bonds.[43,44]

Figure 4 shows that the topography of PEI/NR and PAH/NRLbL films is similar, with round shaped aggregates that increase in size as the number of bilayers increased. Interestingly, cavity-like structures were also formed, which should be expected for films made only with spherical particles.[45,46] For films containing non-particle layers, as those investigated here, the formation of cavities depends on the relationship between particle size

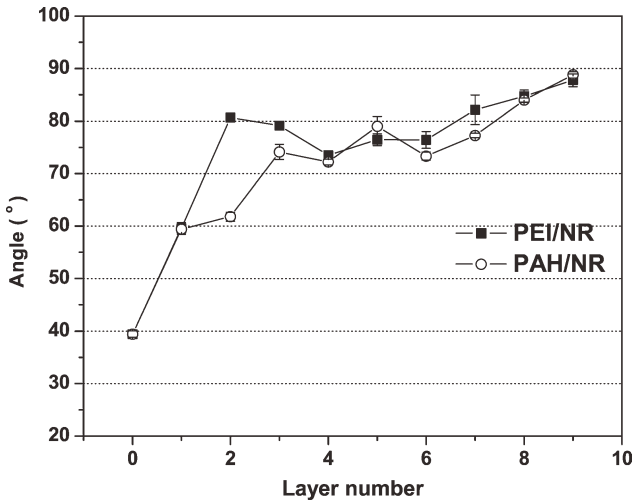

Figure 7 Contact angle measurements on $(PEI/NR)_n$ and $(PAH/NR)_n$ films where n is the number of deposition cycles. Odd numbers represent PEI or PAH at the topmost layer, while latex were in the uppermost layer for even numbers.

and thickness of the polyelectrolyte layer.[47] For these layers may suffer deformation around the particles depending on the layer thickness and particle size.[48]

Consistent with the SEM data, Figure 5 shows AFM images indicating that the size of aggregates increased with the number of bilayers, as it occurred with the film roughness (results not shown). In addition, using the Gwyddion software, we estimated the films mean particle size, volume, and percentage of surface coverage, whose results are shown in Table II. The sizes of the particles were similar, but the surface coverage differed for $(PAH/NR)_5$ and $(PEI/NR)_5$, which may be due to the larger number of particles in the first film. All these values increased as expected for the 15-bilayer LbL films. It is inferred that higher surface coverage is obtained with latex particles for an increasing number of layers, which also increases roughness. The fact that the particle size is uniform in Figure 4 for 5-bilayer LbL films indicates that PEI and PAH layers did not sustain larger particles, which were probably removed during the rinsing step. The larger particles on the 15-bilayer films imply that the deposition of particles (small or big) preferentially happen on top of a previously deposited particle. The line profiles for six particles chosen randomly are shown in Figure 6(a,b), featuring similar shapes for (PAH/NR) with 5 and 15 bilayers. However, the profiles revealed that $(PEI/NR)_5$ films have flat NR particles with width 20 times the maximum height in the center of the particle, in contrast to the particles of the $(PAH/NR)_5$ films (see Fig. 6a).

The differences in morphology for 5-bilayer LbL films made with the different polyammonium salts are worth noting. Both PEI and PAH have amino groups that can be protonated upon varying the pH. However, the branched PEI is known to contain three types of amino groups: secondary and tertiary amino groups in the main chain and secondary and primary amino groups in the side chain, while PAH contains only primary amino groups in the main chain. The amount of nitrogen is therefore 27.73% for PEI and 18.89% for PAH. This difference may lead to distinct strengths of electrostatic attraction between the polymers and the latex particles, thus causing aggregation to differ, also affecting the particles morphology in the first bilayers. The data obtained here, however, are not sufficient to confirm this hypothesis, for which further studies would be required.

The influence from surface roughness on the contact angle is notorious,[49,50] and surface irregularities cause heterogeneous wetting.[50,51] The hydrophilic glass substrates used in this work became increasingly hydrophobic with the deposition of PEI/NR and PAH/NR films, as shown in Figure 7. After a steep increase in contact angle for the first few layers, there was a trend to saturate at 80–90°. The larger increase in angle for the PEI/NR LbL films should be attributed to the larger amount of material adsorbed in the initial cycles (cf. Fig. 1).

Cell growth on NR-containing LbL films

The data for NHF proliferation on LbL and cast films are shown in Table III and Figure 8, where the

TABLE III
NHF Cells Quantification with MTT assays

	7th day			14th day			21st day		
Samples	NHF cells number	SD	Significance	NHF cells number	SD	Significance	NHF cells number	SD	Significance
NR	64,850	± 2911	–	124,700	± 8383	–	35,470	± 14,410	–
PEI	2290	± 240	<0.05	3539	± 240	<0.05	1040	± 240	<0.05
PAH	49,980	± 5582	–	23,920	± 11,100	<0.05	415	± 239	<0.05
$(PEI/NR)_5$	20,410	± 1770	<0.05	20,870	± 448	<0.05	24,300	± 1695	<0.05
$(PAH/NR)_5$	153,500	± 4212	<0.05	186,200	± 11,600	<0.05	90,380	± 6422	<0.05
Control	63,210	± 1195		107,900	± 2026		63,520	± 961	

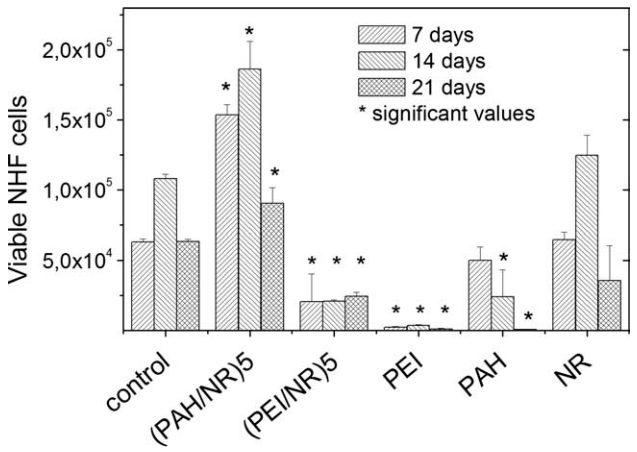

Figure 8 Number of viable NHF cells cultivated in nine replicates over the samples for 7, 14, and 21 days and assessed in MTT assays. The asterisks identify the samples with statistically significant values (*t*-Student test assuming $P < 0.05$) in comparison with the control.

control polystyrene surfaces were taken as reference. The $(PAH/NR)_5$ LbL films were the only ones to exhibit a more efficient cell growth than the control surfaces. The proliferation decreased with time, as also shown in Figure 8.

The morphology of the fibroblasts is shown in the optical images of Figure 9. Analogously to the control surfaces (polystyrene), the $(PAH/NR)_5$ LbL films and the NR cast films displayed the typical elongated morphology. In contrast, the fibroblasts grown on $(PEI/NR)_5$ LbL films and on PEI cast films had atypical shape. On the PAH cast films, a few NHF cells could be seen with the expected morphology of viable cells. This means that the cells could adhere to the PAH surface, but their development was precluded by other factors, such as absence of proteins that assist the surface adhesion or the inadequate conformation of these proteins. Further analysis of cell morphology was made with SEM, and

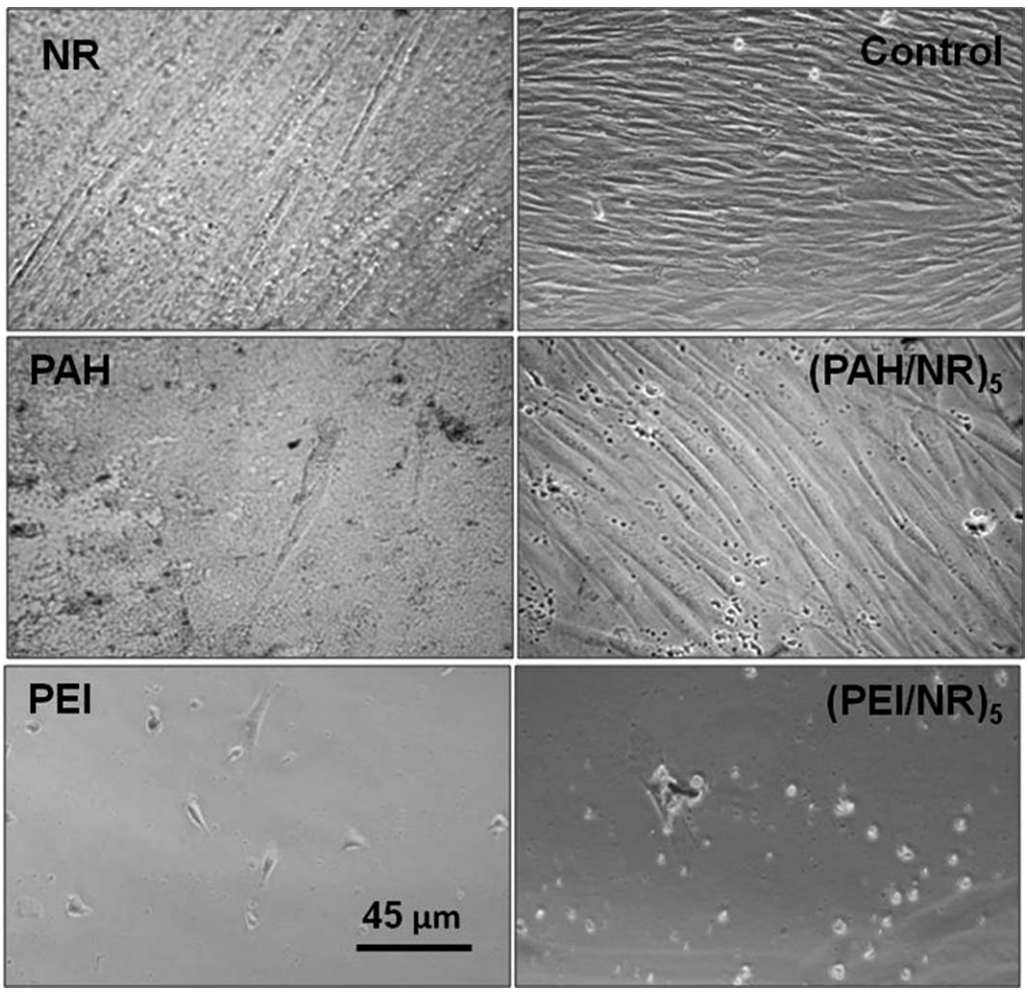

Figure 9 Optical microscopy images of NHF cells cultivated on PEI, PAH, and NR cast films, and on $(PEI/NR)_5$ and $(PAH/NR)_5$ LbL films for 14 days.

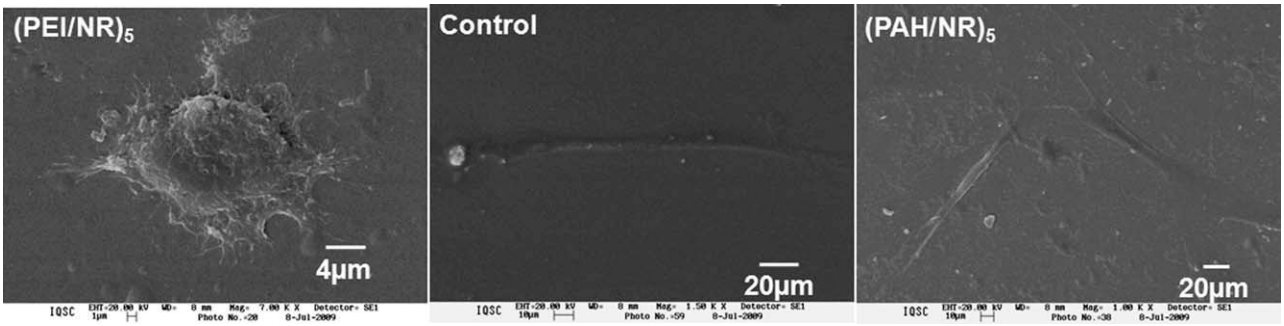

Figure 10 SEM images of NHF cells cultivated during 72 h on the control surface and on $(PEI/NR)_5$ and $(PAH/NR)_5$ LbL films.

the images in Figure 10 reveal that the fibroblasts seem to be flattened on $(PEI/NR)_5$ films, with contours not entirely distinguishable from the substrate and without the typical spreading on a preferential direction. NHF seeded on $(PAH/NR)_5$ films and control surfaces were, on the other hand, able to develop quite well. As NHF needs from 12 to 20 h to adhere and spread on a surface,[48] only cells in advanced stages of spreading and proliferation were expected. Therefore, morphological differences in the optical and electron microscopy analyses can be due to problems of cell adhesion on the multilayer films. The latter may be related to the flat characteristic for the particles in $(PEI/NR)_5$ films.

Two main conclusions can be drawn from the results of LbL and cast films: (i) NR has better performance in LbL than in cast films; (ii) its effects over the NHF proliferation and morphology can be deleterious or beneficial depending on whether LbL films are made in conjunction with PEI or PAH, respectively. The better performance of $(PAH/NR)_5$ LbL films is even more important considering that the content of NR was lower than in the cast films. This piece of information was obtained from an approximate estimate, as follows. The total amount of NR in the cast films was 0.25 μL on each culture well, 35% of which were NR leading to 0.087 μL. This NR was dispersed in the culture well (diameter of 16 mm or 50.3 mm^2) which led to a volume of 1.73 $\mu m^3/\mu m^2$. In the $(PAH/NR)_5$ film, the amount of rubber can be inferred using the AFM images. The volume of the particles (138 μm^3) in an area of 50×50 μm, as used for the AFM data, gives merely 0.06 $\mu m^3/\mu m^2$ of rubber in the LbL films.

While a more suitable surface could be expected for the LbL films in comparison with cast films,[24–27,52] the differences between $(PAH/NR)_n$ and $(PEI/NR)_n$ films were surprising because the latter films exhibited similar physicochemical characteristics, in terms of adsorption, stability, and wettability morphology. Moreover, both PAH and PEI are considered as biocompatible materials. A possible explanation for the enhanced cell growth in the PAH-containing films may be the higher charge density of PEI, with its larger number of protonated amino groups (see Fig. 11). An excessive tension could be caused on the cell membranes on $(PEI/NR)_5$ films, thus hampering development. On the other hand, differences in surface charge led to only small differences in cell viability for silica nanoparticles coated with LbL films containing PEI and PAH.[53] The inevitable conclusion is then that the flattening of the particles appears to be the most probable reason for the lower cell proliferation on $(PEI/NR)_5$ films, as already discussed, which would be an indirect consequence of the higher charge density of PEI.

It is stressed that a major limitation of the approach adopted here is that the experiments were performed far from the real biological conditions in living beings. Nevertheless, it is also true that breakthroughs in functionalized surfaces for real applications (e.g., for tissue engineering) can only be made if basic understanding is available on the cell growth on functionalized surfaces. Therefore, the clear advantage of surfaces modified with special architectures of LbL films demonstrated here is the first step for further developments toward real biological applications.

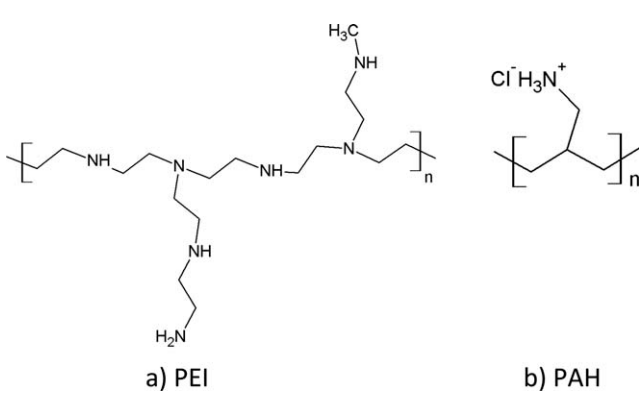

Figure 11 Molecular structure of a) PEI e b) PAH.

CONCLUSION

The viability of adsorbing LbL films from natural rubber latex (NR) on different types of solid substrates was demonstrated for two polycations, namely PEI and PAH. While the multilayer $(PEI/NR)_n$ and $(PAH/NR)_n$ films had similar physicochemical characteristics, including wettability and film growth properties, their morphology differed considerably. Of particular relevance was that the $(PEI/NR)_5$ LbL films contained flattened particles that were not efficient for growth and proliferation of normal human fibroblasts (NHF). The multilayer $(PAH/NR)_n$ films, in contrast, induced fibroblasts proliferation with the typical elongated morphology. These differences for the two similar polycations are probably related to the distinct degrees of charging, thus pointing to the importance of a precise control in molecular and film architectures. In a comparative study, we noted that cell growth did not occur on NR cast films, which again demonstrates the advantages of the LbL methods for biologically related applications. In summary, the findings reported here highlight the need to obtain molecular level information on functionalized surfaces, whose ability to sustain cell growth may vary widely depending on the surface properties, including morphology. In addition, we have shown that further applications may be sought for NR, now taking advantage of the molecular control afforded in LbL films.

This work was supported by UFABC, FAPESP, CNPq, Capes, and Rede nBioNet (Brazil).

References

1. Chopra, V.; Peter, K. Handbook of Industrial Crops; CRC Press: Boca Raton, 2005.
2. Mrué, F.; Netto, J. C.; Ceneviva, R.; Lachat, J. J.; Thomazini, J. A.; Tambelini, H. Mater Res Ibero-Am J Mater 2004, 7, 277.
3. Frade, M. A. C.; Valverde, R. V.; de Assis, R. V. C.; Coutinho-Netto, J.; Foss, N. T. Int J Dermatol 2001, 40, 238.
4. Balabanian, C. A. C. A.; CoutinhoNetto, J.; Lamano-Carvalho, T. L.; Lacerda, S. A.; Brentegani, L. G. J Oral Sci 2006, 48, 201.
5. Herculano, R. D.; Guimaraes, S. A. C.; Belmonte, G. C.; Duarte, M. A. H.; de Oliveira, O. N.; Kinoshita, A.; Graeff, C. F. D. Mater Res-Ibero-Am J Mater 2010, 13, 57.
6. Ferreira, M.; Mendonca, R. J.; Coutinho-Netto, J.; Mulato, M. Brazil J Phys 2009, 39, 564.
7. Herculano, R. D.; Silva, C. P.; Ereno, C.; Guimaraes, S. A. C.; Kinoshita, A.; Graeff, C. F. D. Mater Res-Ibero-Am J Mater 2009, 12, 253.
8. Herculano, R. D.; Brunello, C. A.; Graeff, C. F. O. Macromol Symp 2006, 245–246, 529.
9. Neves, W. F. P.; Graeff, C. F. D.; Ferreira, M.; Mulato, M.; Bernardes, M. S.; Coutinho-Netto, J. J Appl Polym Sci 2006, 100, 702.
10. Neves-Junior, W. F. P.; Ferreira, M.; Alves, M. C. O.; Graeff, C. F. O.; Mulato, M.; Coutinho-Netto, J.; Bernardes, M. S. Brazil J Phys 2006, 36, 586.
11. Coutinho, J.; Mrue, F.; Pele Nova Biotecnologia Sa. WO2005008932-A2; Coutinho, J.; Mrue, F.;US2005049331-A1, 2005.
12. Mrue, F.; Pele Nova Biotecnologia Sa.BR200405995-A, 2006.
13. Mrue, F.; Pele Nova Biotecnologia Sa; WO2007048215-A1; Mrue, F.; BR200504797-A; Mrue, F.; EP1951185-A1; Mrue, F.; US2008279885-A1; Mrue, F.; JP2009513581-W,2007.
14. Mrue, F.; Coutinho, J.; Pele Nova Biotecnologia Sa. WO2007059597-A2; Mrue, F.; Coutinho, J.; BR200506041-A; Mrue, F.; Coutinho, J.; EP1963356-A2; Mrue, F.; Coutinho, J.; US2009093404-A1, 2007.
15. Mrue, F.; Pele Nova Biotecnologia Sa.WO2009155678-A1, 2010.
16. Palosuo, T.; Lehto, M.; Kotovuori, A.; Kalkkinen, N.; Blanco, C.; Poza, P.; Carrillo, T.; Hamilton, R. G.; Alenius, H.; Reunalak, T.; Turjanmaa, K. Clin Exp Allergy 2007, 37, 1502.
17. Yeang, H. Y.; Hamilton, R. G.; Bernstein, D. I.; Arif, S. A. M.; Chow, K. S.; Loke, Y. H.; Raulf-Heimsoth, M.; Wagner, S.; Breiteneder, H.; Biagini, R. E. Clin Exp Allergy 2006, 36, 1078.
18. Sussman, G. L.; Beezhold, D. H. Ann Int Med 1995, 122, 43.
19. Guarneri, F.; Guarneri, C.; Guarneri, B.; Benvenga, S. Clin Exper Allergy 2006, 36, 916.
20. Raulf-Heimsoth, M.; Rihs, H. P.; Rozynek, P.; Cremer, R.; Gaspar, A.; Pires, G.; Yeang, H. Y.; Arif, S. A. M.; Hamilton, R. G.; Sander, I.; Lundberg, M.; Bruning, T. Clin Exper Allergy 2007, 37, 1657.
21. Alenius, H.; Kalkkinen, N.; Lukka, M.; Reunala, T.; Turjanmaa, K.; Makinenkiljunen, S.; Yip, E.; Palosuo, T. Clin Exper Allergy 1995, 25, 659.
22. Mendonca, R. J.; Mauricio, V. B.; Teixeira, L. D.; Lachat, J. J.; Coutinho-Netto, J. Phytother Res 2010, 24, 764.
23. Decher, G. Science 1997, 277, 1232.
24. Wittmer, C. R.; Phelps, J. A.; Lepus, C. M.; Saltzman, W. M.; Harding, M. J.; Van Tassel, P. R. Biomaterials 2008, 29, 4082.
25. Cai, K. Y.; Wang, Y. L. J Mater Sci-Mater Med 2006, 17, 929.
26. Chen, J. L.; Chen, C.; Chen, Z. Y.; Chen, J. Y.; Li, Q. L.; Huang, N. J Biomed Mat Res Part A 2010, 95A, 341.
27. Kadowaki, K.; Matsusaki, M.; Akashi, M. Langmuir 2010, 26, 5670.
28. Zhou, J.; Romero, G.; Rojas, E.; Ma, L.; Moya, S.; Gao, C. Y. J Colloid Interf Sci 2010, 345, 241.
29. Fukuda, J.; Khademhosseini, A.; Yeh, J.; Eng, G.; Cheng, J. J.; Farokhzad, O. C.; Langer, R. Biomaterials 2006, 27, 1479.
30. Mendelsohn, J. D.; Yang, S. Y.; Hiller, J.; Hochbaum, A. I.; Rubner, M. F. Biomacromolecules 2003, 4, 96.
31. Erol, M.; Du, H.; Sukhishvili, S. Langmuir 2006, 22, 11329.
32. Mao, Z. W.; Ma, L.; Zhou, J.; Gao, C. Y.; Shen, J. C. Bioconjug Chem 2005, 16, 1316.
33. Wen, J.; Arakawa, T.; Philo, J. S., Anal Biochem 1996, 240, 155.
34. Rajangam, K.; Behanna, H. A.; Hui, M. J.; Han, X. Q.; Hulvat, J. F.; Lomasney, J. W.; Stupp, S. I. Nano Lett 2006, 6, 2086.
35. Morton, M. Rubber Technology; Van Nostrand Reinhold: New York, 1987.
36. d'Auzac, J.; Jacob, J.-L.; Chrestin, H. Physiology of Rubber Tree Latex; CRC Press: Boca Raton, 1989.
37. Rippel, M. M.; Lee, L. T.; Leite, C. A. P.; Galembeck, F. J Colloid Interf Sci 2003, 268, 330.
38. Wood, K. C.; Boedicker, J. Q.; Lynn, D. M.; Hammon, P. T. Langmuir 2005, 21, 1603.
39. Predeep, P.; Sreeja, R.; Mazur, M.; Sharma, P. J Elastomers Plastics 2006, 38, 333.
40. Healey, A. M.; Hendra, P. J.; West, Y. D. Polymer 1996, 37, 4009.
41. Yang, T.; Hussain, A.; Bai, S.; Khalil, I. A.; Harashima, H.; Ahsan, F. J Control Release 2006, 115, 289.
42. Crespilho, F. N.; Zucolotto, V.; Siqueira, J. R.; Constantino, C. J. L.; Nart, F. C.; Oliveira, O. N. Environ Sci Technol 2005, 39, 5385.
43. Raposo, M.; Oliveira, O. N. Braz J Phys 1998, 28, 392.
44. Lavalle, P.; Gergely, C.; Cuisinier, F. J. G.; Decher, G.; Schaaf, P.; Voegel, J. C.; Picart, C. Macromolecules 2002, 35, 4458.

45. Adamczyk, Z.; Weronski, P.; Barbasz, J.; Kolasinska, M. Appl Surf Sci 2007, 253, 5776.
46. Adamczyk, Z.; Weronski, P.; Barbasz, J. J Colloid Interf Sci 2008, 317, 1.
47. Sangribsub, S.; Tangboriboonrat, P.; Pith, T.; Decher, G. Euro Polym J 2005, 41, 1531.
48. Volodkin, D.; Arntz, Y.; Schaaf, P.; Moehwald, H.; Voegel, J. C.; Ball, V. Soft Matter 2008, 4, 122.
49. Israelachvili, J. Intermolecular & Surface Forces; Academic Press: EUA, 1991.
50. Marmur, A. Langmuir 2004, 20, 3517.
51. Hikita, M.; Tanaka, K.; Nakamura, T.; Kajiyama, T.; Takahara, A. Langmuir 2005, 21, 7299.
52. Ferreira, M.; Zucolotto, V.; Mulato, M.; Oliveira Jr, O.N., NSTI Nanotech, 2006, Boston. Technical Proceedings of the 2006 NSTI Nanotechnology Conference and Trade Show. Cambridge, MA, USA: Nano Science & Technology Institute, 2006.v. 2. p.129–132.
53. Liu, G.; Tian, J.; Liu, C.; Ai, H.; Gu, Z. W.; Gou, J. L.; Mo, X. M. J Mater Res 2009, 24, 1317.